# CW-EPR spectrometer

Waveguides bring μwave beam into and out of cavity, and to detector

Electronics, frequency and phase selective amplifier, recorder/computer

detector crystal

Various designs of cavity to provide optimal coupling of μwave energy, magnetic field flux, etc.

klystron μwave source, - provides fixed frequency

Oscilloscope

*Source*

Terminating load

Circulator or hybrid tee

Isolator

Attenuator

*Detection system*

Wavemeter

100 kHz signal amplifier

100 kHz signal detector

Recorder

μA

Klystron power supply

Slide screw turner

magnetic field flux in x,y-plane

Resonant cavity

*Magnet system*

Iris

Electromagnet

Automatic frequency control

Magnet power supply

A

100 kHz modulation coils

C

Magnet provides main field. Field can be varied over range of interest using field scan drive

Field scan drive

100 kHz power amplifier

100 kHz oscillator

*Modulation system*

modulation coils modulate magnetic field at 100 kHz

$m_S=+1/2$

E

$\Delta E = g_e \beta B = h\nu$

Photon Energy

$m_S=-1/2$

$B_R$

B

Absorption

B

$\dfrac{dA}{dB}$

B

B

**S**

(when $m_S = +1/2$)

**S**

($m_S = -1/2$)

large **μ**

small **μ**

E

$h\nu$

"free electron"

B

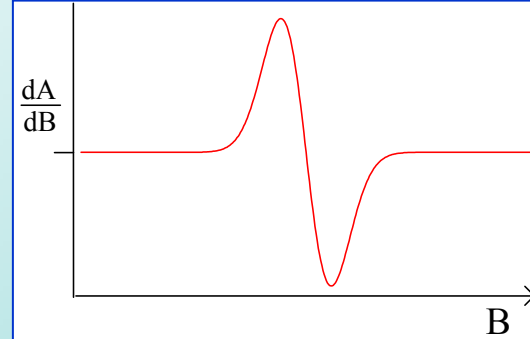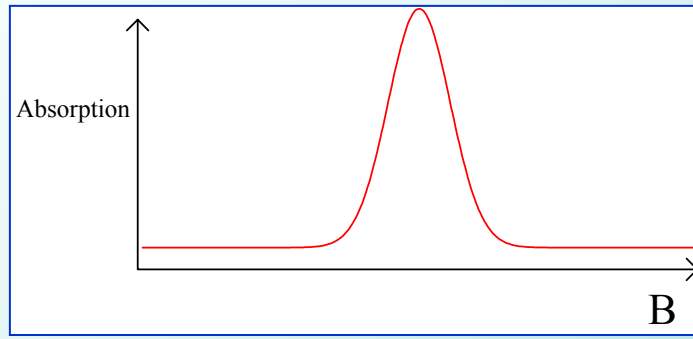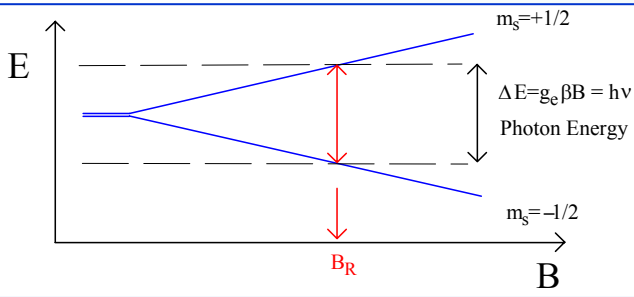angular momentum from ORBITAL
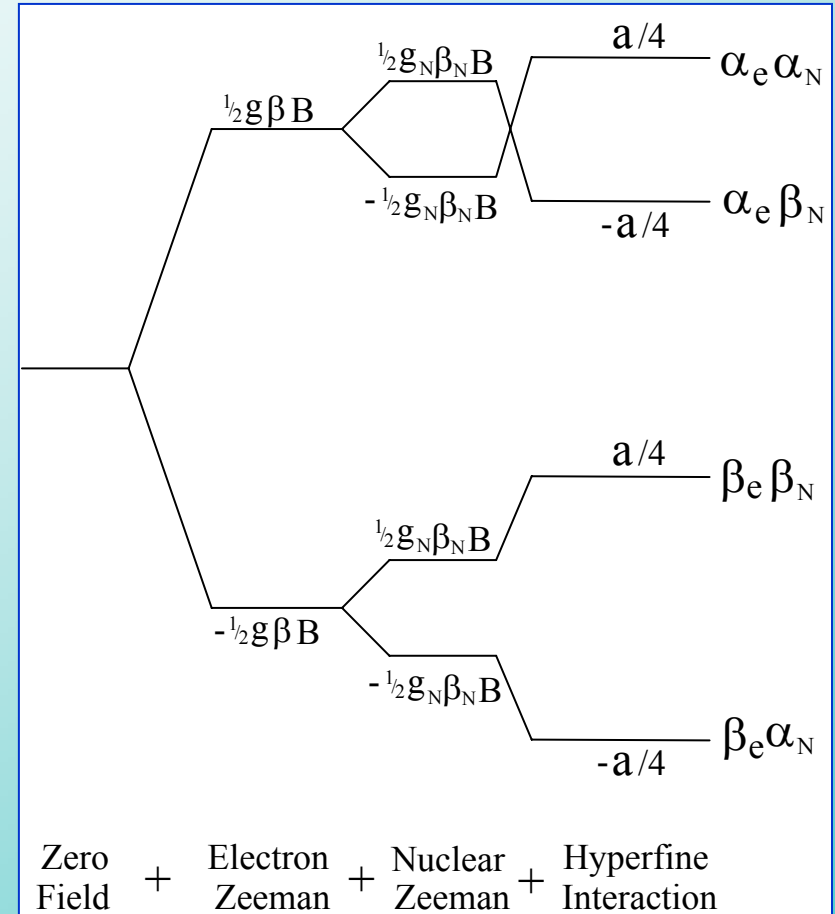
**l**

angular momentum from SPIN

**s**

$e^-$

Electrons in molecules are in *orbitals*.  In these orbitals they move around their own nucleus and through conjugate bonds.  This motion leads to a second type of angular momentum for the electron, *orbital angular momentum*, given the symbol **l**.  Again the combination of angular momentum and charge create a magnetic moment for the electron.  This second contribution to the electron's magnetic moment can add to or subtract from the first.  Thus the total magnetic moment and therefore the $g_{obs}$-value can rise or fall relative to $g_e$.

In addition to the spin coupling between magnetic effects arising from spin and orbital angular momentum contributions, the electron spin is also modified by interaction with local nuclear spins. This is called hyperfine interaction.

The magnetic field produced by the nucleus either adds to or subtracts from the imposed magnetic field. Consequently, the electron can experience two different **local** (atomic or molecular) magnetic fields. The single EPR line which would be observed when there is no hyperfine interaction is shifted to higher or lower energy depending on the nuclear spin orientation in a particular atom.



$\frac{1}{2}g_N\beta_N B$     $a/4$     $\alpha_e \alpha_N$

$\frac{1}{2}g\beta B$

$-\frac{1}{2}g_N\beta_N B$     $-a/4$     $\alpha_e \beta_N$

$a/4$     $\beta_e \beta_N$

$\frac{1}{2}g_N\beta_N B$

$-\frac{1}{2}g\beta B$

$-\frac{1}{2}g_N\beta_N B$

$-a/4$     $\beta_e \alpha_N$

Zero Field   +   Electron Zeeman   +   Nuclear Zeeman   +   Hyperfine Interaction

**Origin of g-value Anisotropy**

Shifts of the g-value from $g_e$=2.0023 occur when the unpaired electron acquires **orbital angular momentum** in addition to intrinsic **spin angular momentum**.

An unpaired electron in a molecular orbital can acquire an orbital moment because it may be free to undergo "rotation" about one of the axes (for example, one unpaired electron in a set of degenerate d-orbitals). Because the orbitals are degenerate, the unpaired electron is distributed equally amongst the different atomic orbitals. It can be viewed as moving through all the orbitals and effectively undergoing rotation about any axis.

**Summary of the Contributions to Nuclear Hyperfine Splittings**

The **isotropic** contribution ALWAYS arises from unpaired electron density being directly in or reaching an s-orbital (symmetrical) on the nucleus involved.

The **anisotropic** contribution arises from a through-space dipolar interaction between the unpaired electron and the nucleus. The magnitude and sign vary with the direction of the magnetic field and the type of orbital occupied by the unpaired electron.
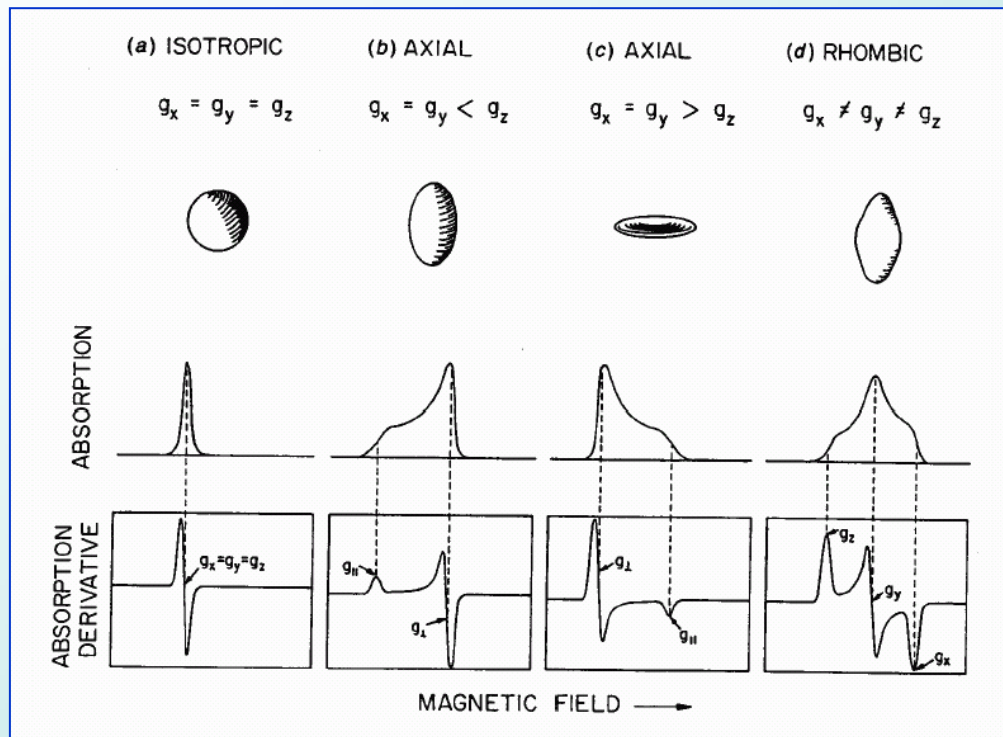
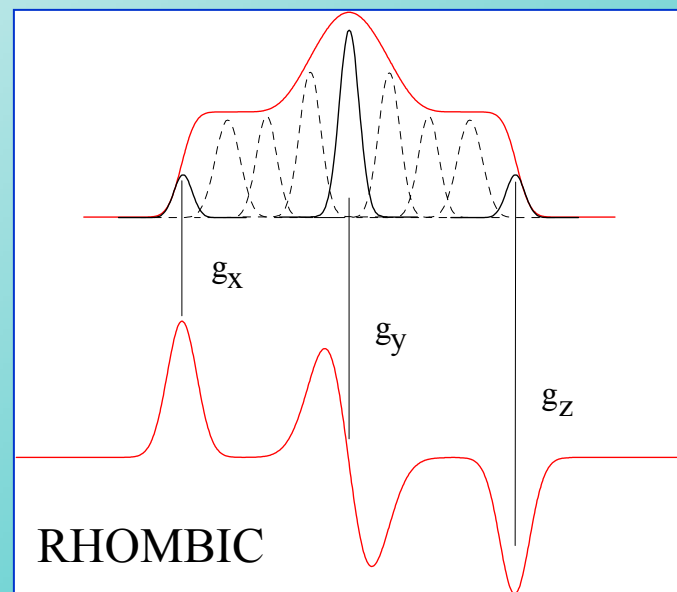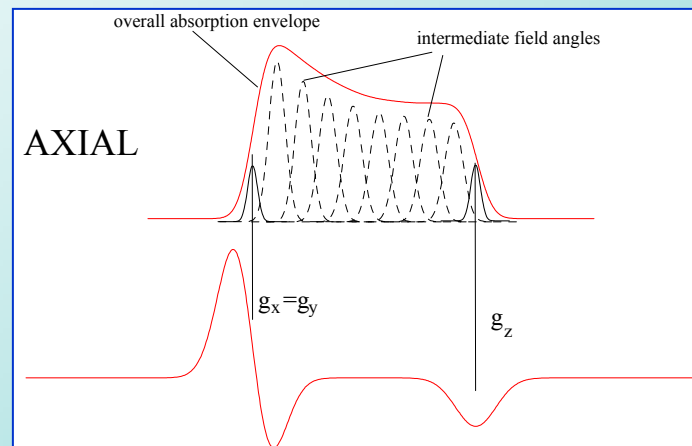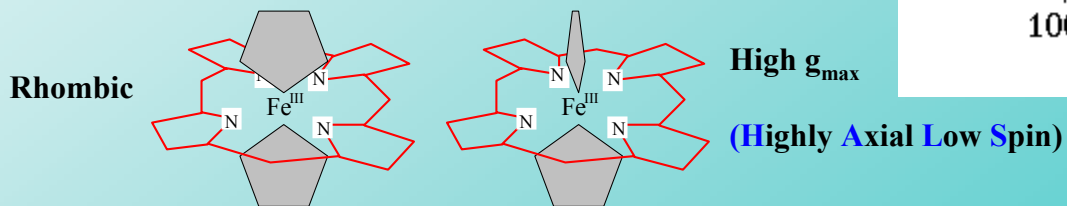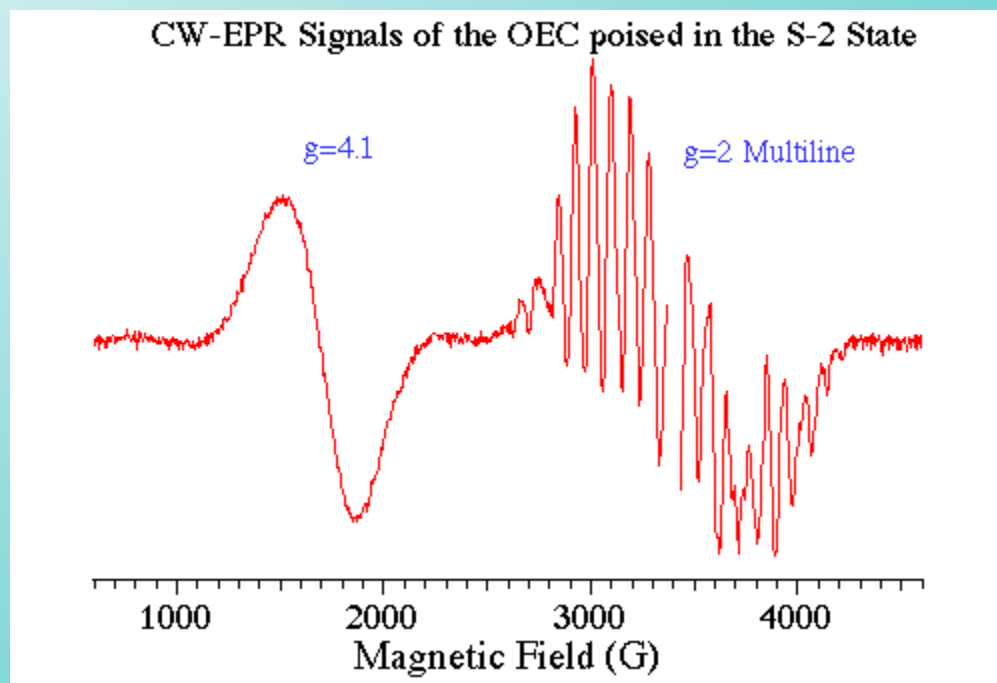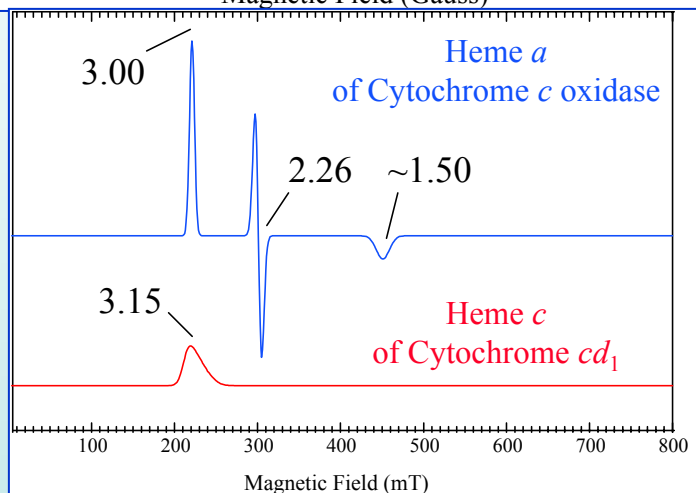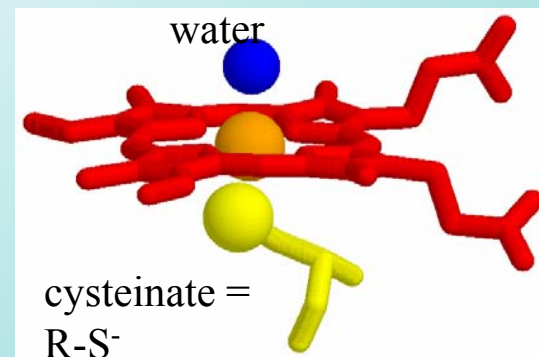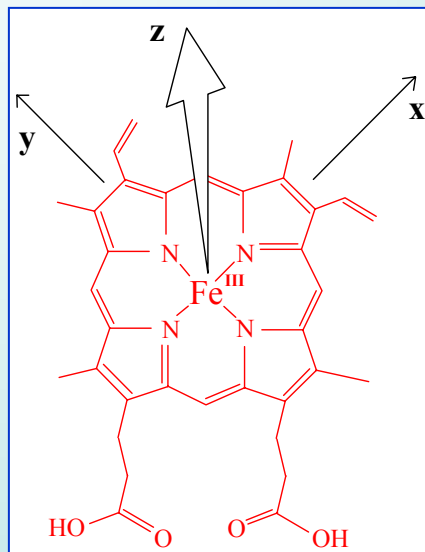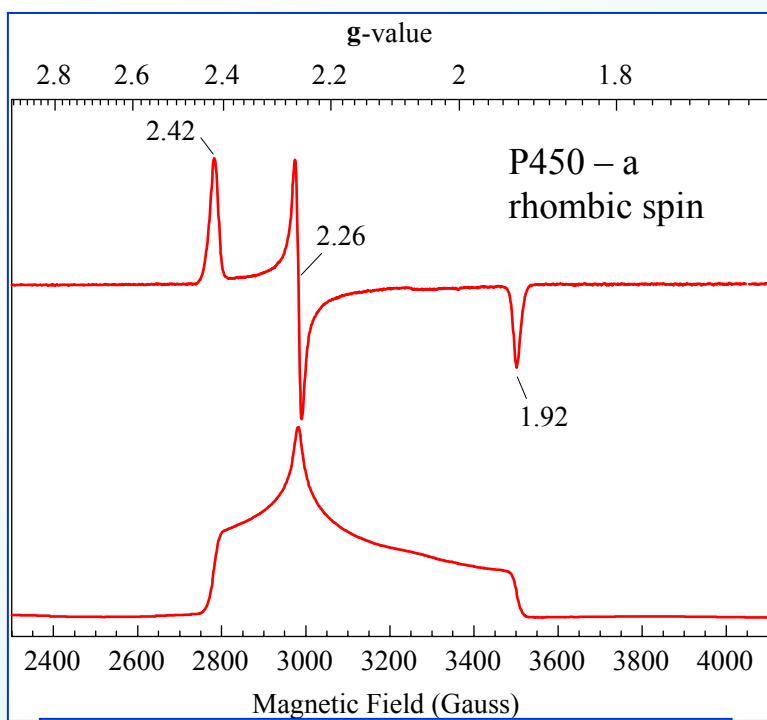Molecular orbitals for the electron give rise to
energy levels that are dependent on orientation, - the
shape of the orbit, and hence the effect of an
external magnetic field, and the energies of spin flip
transitions for electrons in the orbit, varies with
orientation.

In a crystal with only one orientation of the molecule, these different energies would give rise to separate EPR spectral lines.

In a solution, or a frozen "powder" sample, all orientations are selected, so we see the overlap of multiple bands.

As we shall see later, pulse EPR can be used to select a particular orientation by choice of the frequency at which we excite the spin population. For example, by using a pulse at a combination of field strength and microwave frequency that selects the $g_x$ line in a rhombic spectrum, we can select those orientations in which the $g_x$ transitions are favored. The decay of the spin population then reflects the nuclear interactions of that population.



AXIAL

overall absorption envelope    intermediate field angles

$g_x = g_y$    $g_z$



$g_x$    $g_y$    $g_z$

RHOMBIC

**g-value**

2.8   2.6   2.4   2.2   2   1.8

2.42

2.26

P450 – a
rhombic spin

1.92

2400  2600  2800  3000  3200  3400  3600  3800  4000

Magnetic Field (Gauss)

z

y

x

Fe^III

HO   O        O   OH

water

cysteinate =
R-S⁻

3.00

Heme *a*
of Cytochrome *c* oxidase

2.26   ~1.50

3.15

Heme *c*
of Cytochrome *cd*₁

100   200   300   400   500   600   700   800

Magnetic Field (mT)

CW-EPR Signals of the OEC poised in the S-2 State

g=4.1                    g=2 Multiline

1000        2000        3000        4000

Magnetic Field (G)

**Rhombic**

Fe^III          Fe^III

**High g_max**

**(Highly Axial Low Spin)**

## Nitroxide spins as probes of protein environment

Nitroxides have an inherent paramagnetic centre that gives a characteristic three line signal on aqueous solution. Nitroxides have been synthesized with various substituents, and terminal groups appropriate for attachment to cysteine residues. The local environment of an attached NO effects both the spacing between the peaks, and the width of the peaks.

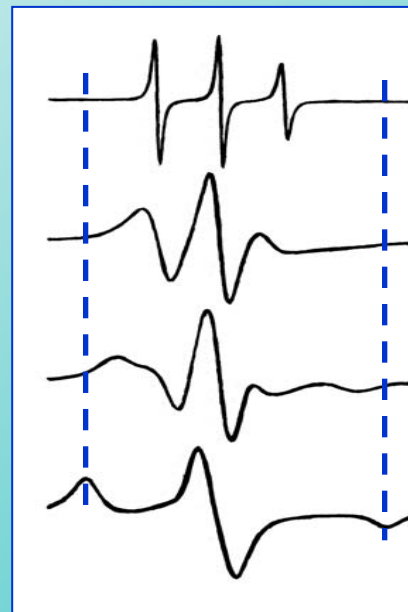The spectra (right) show the effect of environment on the mobility of the probe.

FIGURE 1: Spin-labels **I**, **II**, and **III** and the corresponding side chains R1, R2, and R3.
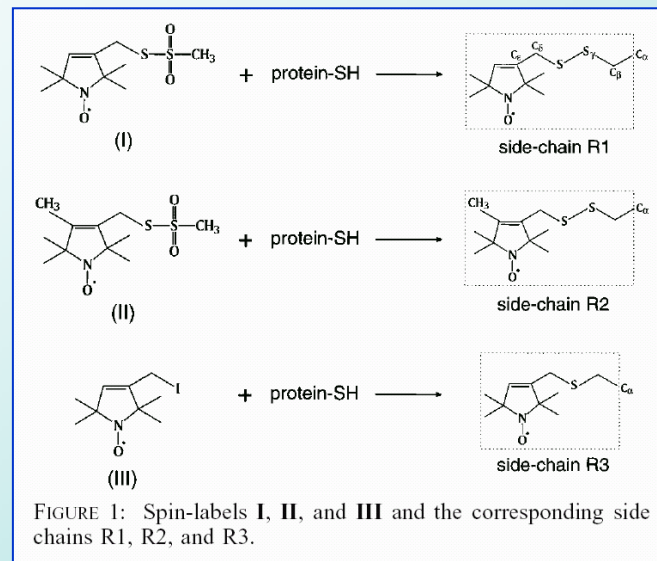
7692                    *Biochemistry* **1996**, *35*, 7692−7704

Motion of Spin-Labeled Side Chains in T4 Lysozyme. Correlation with Protein Structure and Dynamics†

Hassane S. Mchaourab,‡ Michael A. Lietzow,‡ Kalman Hideg,§ and Wayne L. Hubbell*,‡

**fast**

**intermediate**

**slow**

**rigid**

Nitroxide spins in different protein environments.

An extensive study by Hubbell and colleagues of the effect of spin environment when attached at specific sites engineered in lysozyme has provided a diagnostic tool for the study of environment in other proteins. The examples above illustrate the different spectra found in surface and buried locations. The results are summarized in the Fig. at bottom right.
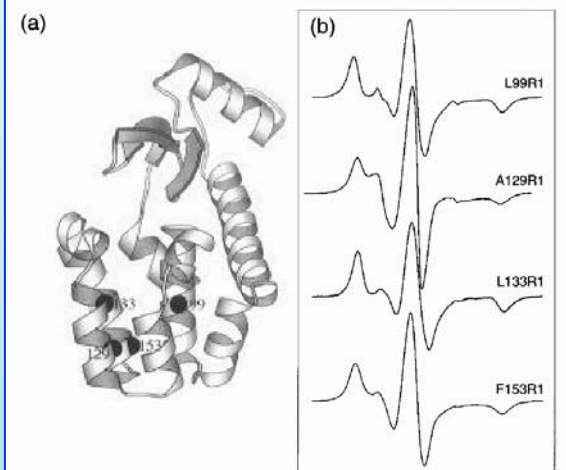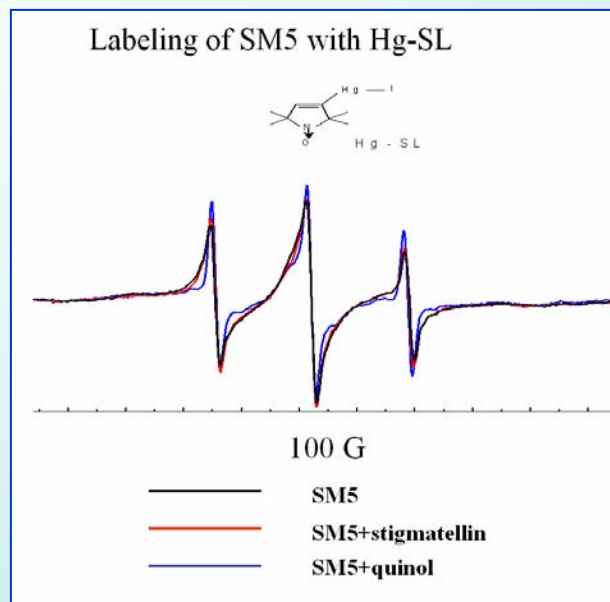


Labeling of SM5 with Hg-SL

100 G

— SM5
— SM5+stigmatellin
— SM5+quinol



FIGURE 11: (a) Crystal structure of T4L showing the location of buried sites. (b) Corresponding EPR spectra of side-chain R1. The magnetic field scan width is 98 G.
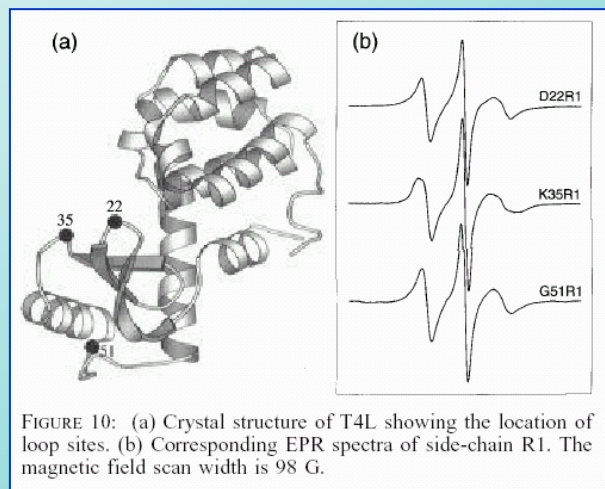


FIGURE 10: (a) Crystal structure of T4L showing the location of loop sites. (b) Corresponding EPR spectra of side-chain R1. The magnetic field scan width is 98 G.
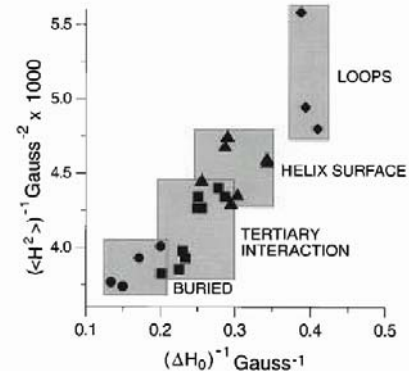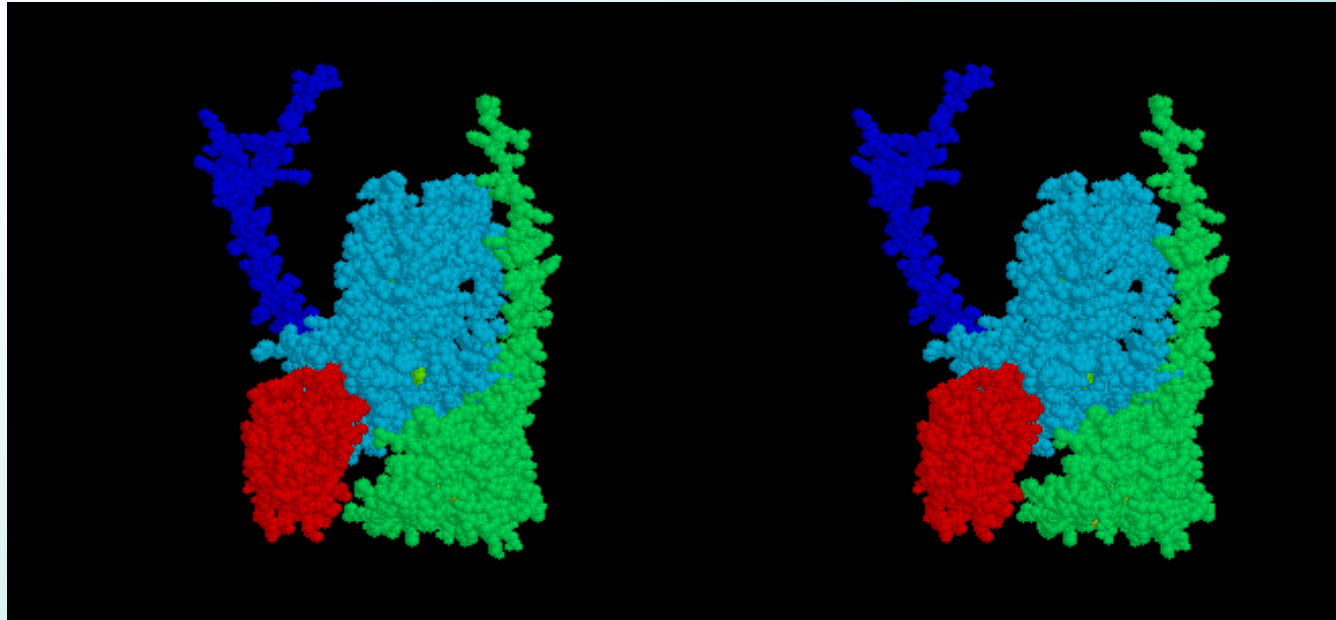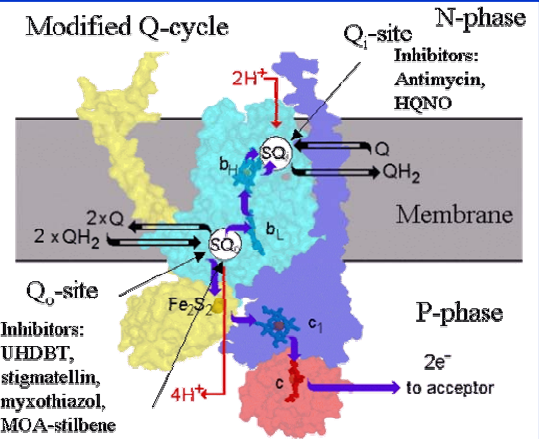


FIGURE 13: Reciprocal second moment versus the reciprocal central line width calculated from the EPR spectra of R1 at the sites shown.

Mechanism of quinol oxidation by the $bc_1$ complex. The ISP interacts with the $Q_o$-site where it is reduced by quinol, and is oxidized by cyt $c_1$



Movement of the ISP to ferry electrons from $Q_o$-site to cyt $c_1$.

Different positions of the ISP found in different crystals. The structure with stigmatellin (yellow ball&stick model) in position 4 has a H-bond between a -C=O group of stigmatellin and one of the His ligands of the ISP [2Fe-2S] cluster. This is thought to mimic the interaction of quinone with ISP.
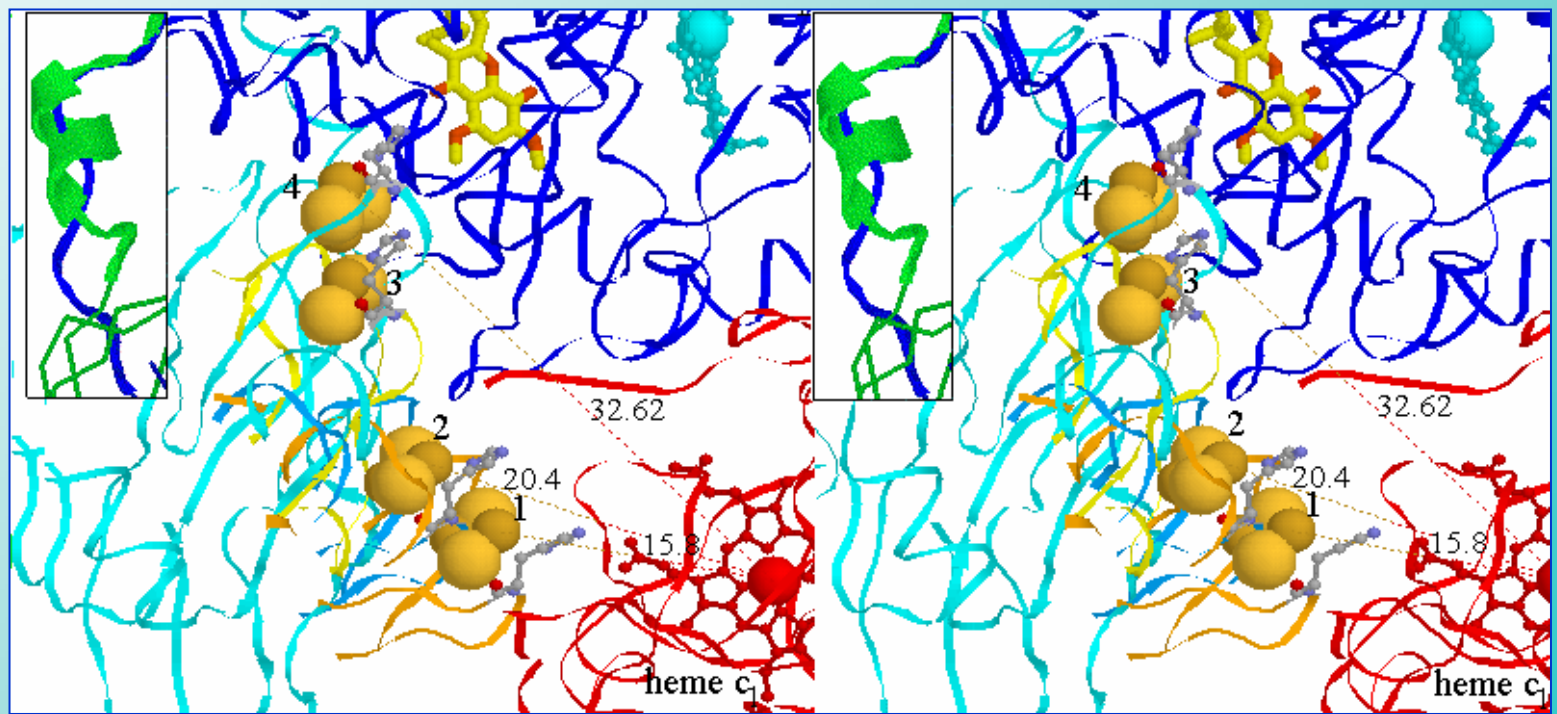
Left: Experiments by de Vries which demonstrated that the sharp $g_x$ line was seen only if the complex contained oxidized quinone and reduced ISP (ascorbate as reductant).

Right: Spectra of the ISP in mutant bacterial strains, showing the $g_x$ band with quinone (top) or with stigmatellin (bottom). Note shifts in $g_x$ position. The mutations were at Tyr-156, which H-bonds to one of the Cys ligands of the [2Fe-2S] cluster. These mutants have modified $E_m$ and pK values. With myxothiazol in the site, the spectrum was like that of the extracted sample.
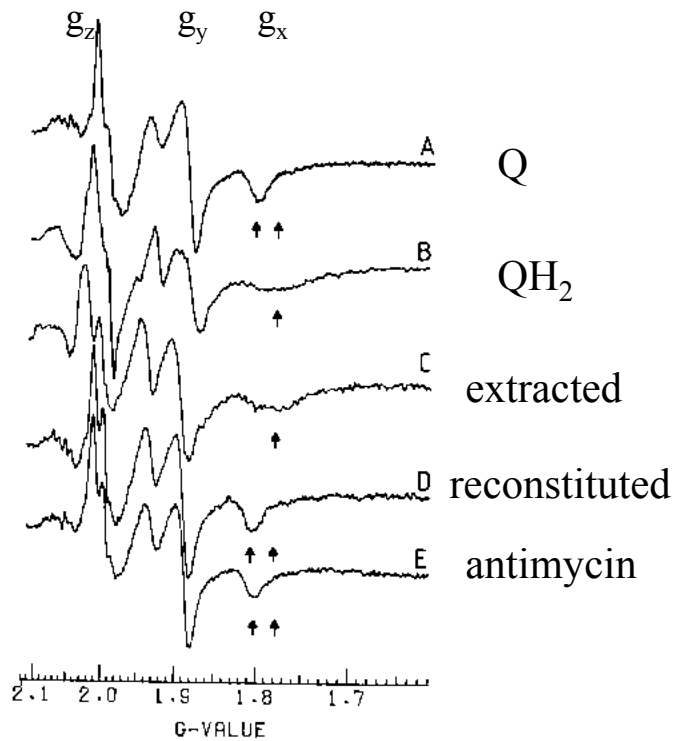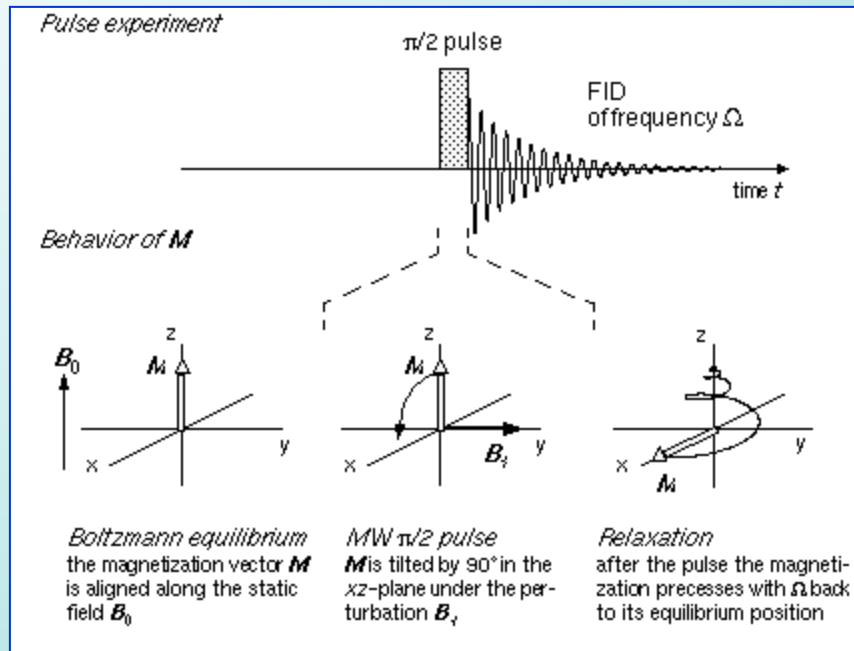
The spectra show a characteristic rhombic form with $g_x$, $g_y$ and $g_z$ lines. The $g_x$ line changes, depending on interactions with the $Q_o$-site occupant.
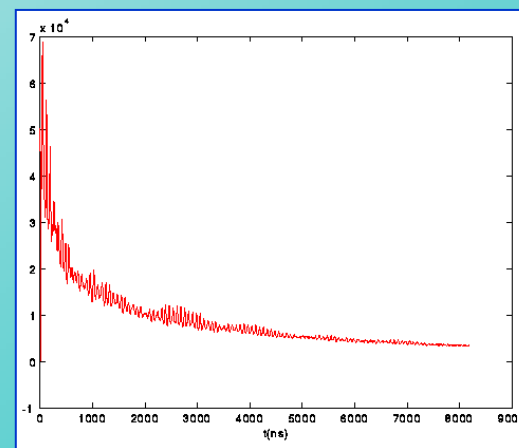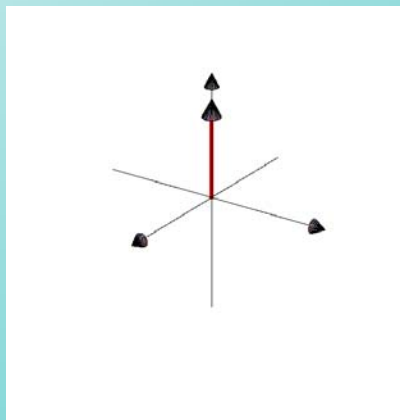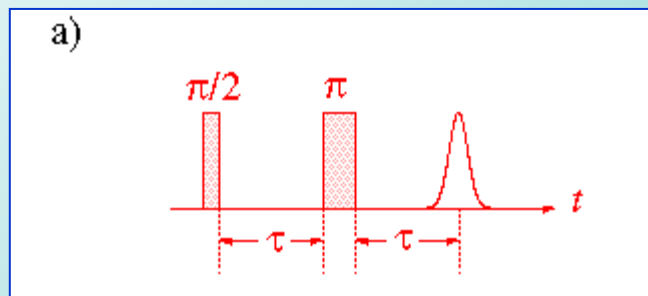


deVries et al. (1982)
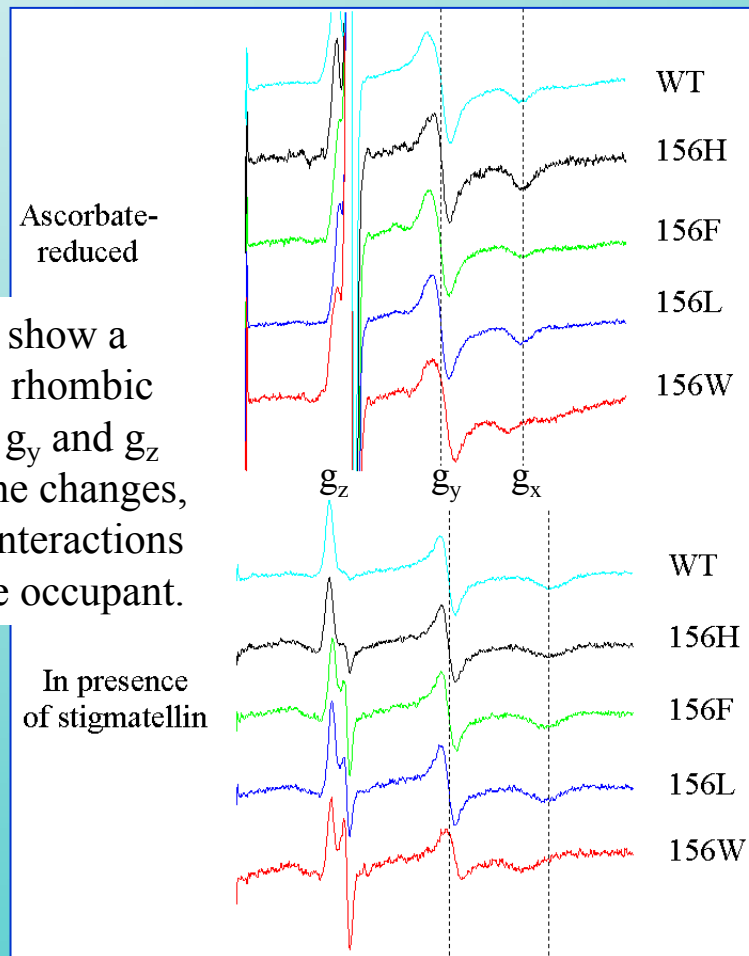
## Pulsed EPR

General principles are the same as for NMR. However, the spectra are generally much simpler because we are sampling interactions between the paramagnetic center and a relatively small number of nuclear spins. The range is about the same as for NOE - ~5 Å. Note that these interactions are often through space (not through bonds), but are structurally linked, as in NOE spectra.



*Pulse experiment*

π/2 pulse

FID of frequency Ω

time *t*

*Behavior of M*

*Boltzmann equilibrium*
the magnetization vector ***M*** is aligned along the static field ***B₀***

*MW π/2 pulse*
***M*** is tilted by 90° in the *xz*-plane under the perturbation ***Bᵧ***

*Relaxation*
after the pulse the magnetization precesses with Ω back to its equilibrium position

Simple two-pulse sequence

Pancake echo

FID from echo



a)

π/2     π

τ    τ

*t*

In pulse EPR, the most popular sequence for the measurement of the nuclear modulation effect is still the primary echo sequence $\pi/2$-$\tau$-$\pi$-$\tau$-echo (a). In the following the pulses are assumed to be ideally non-selective. This means in practice that the two pulses are taken as sufficiently strong and short as possible.

The creation of a primary echo can be understood in the following way. The net magnetization vector is assumed to be initially oriented along the z-axis (b). A $\pi/2$ pulse along x will rotate the magnetization by $90^o$ to the -y-axis (c).

During time $\tau$ between the first and second pulse, the different spin packets freely evolve (dephasing of the different spin packets) (d). The $\pi$ pulse inverts the y-component of the individual magnetization vectors (e). After a time $\tau$, the magnetization vectors are in phase along the +y-axis and a primary echo is observed (f).
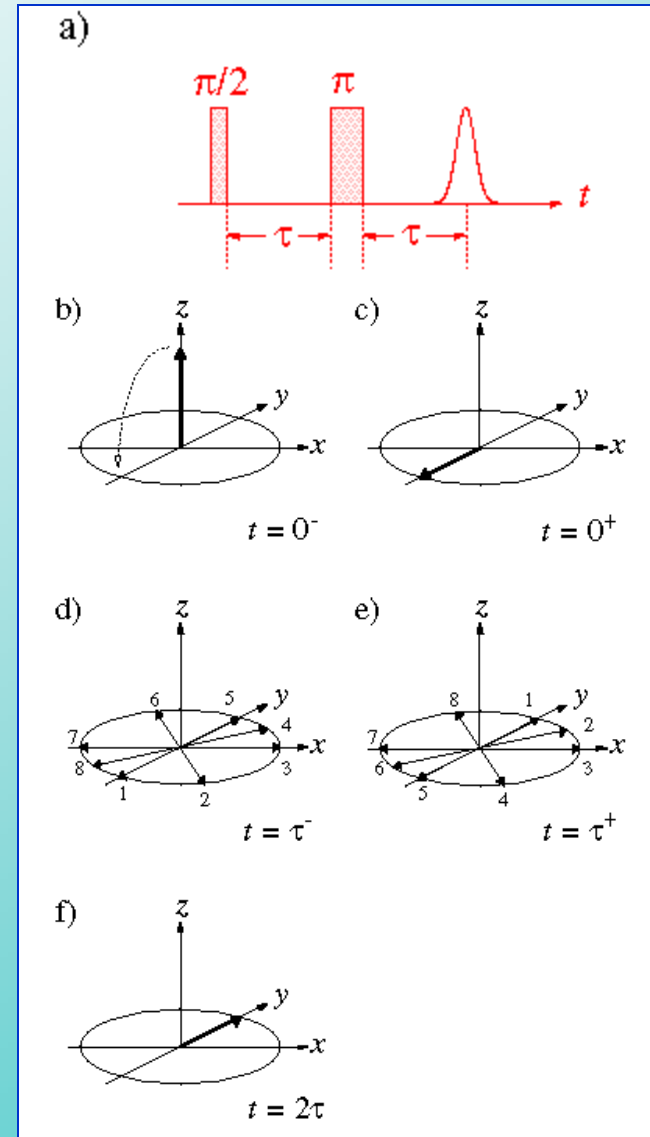
From (c-f) of the previous slide, it can be seen that the primary echo is a "pancake like" echo.
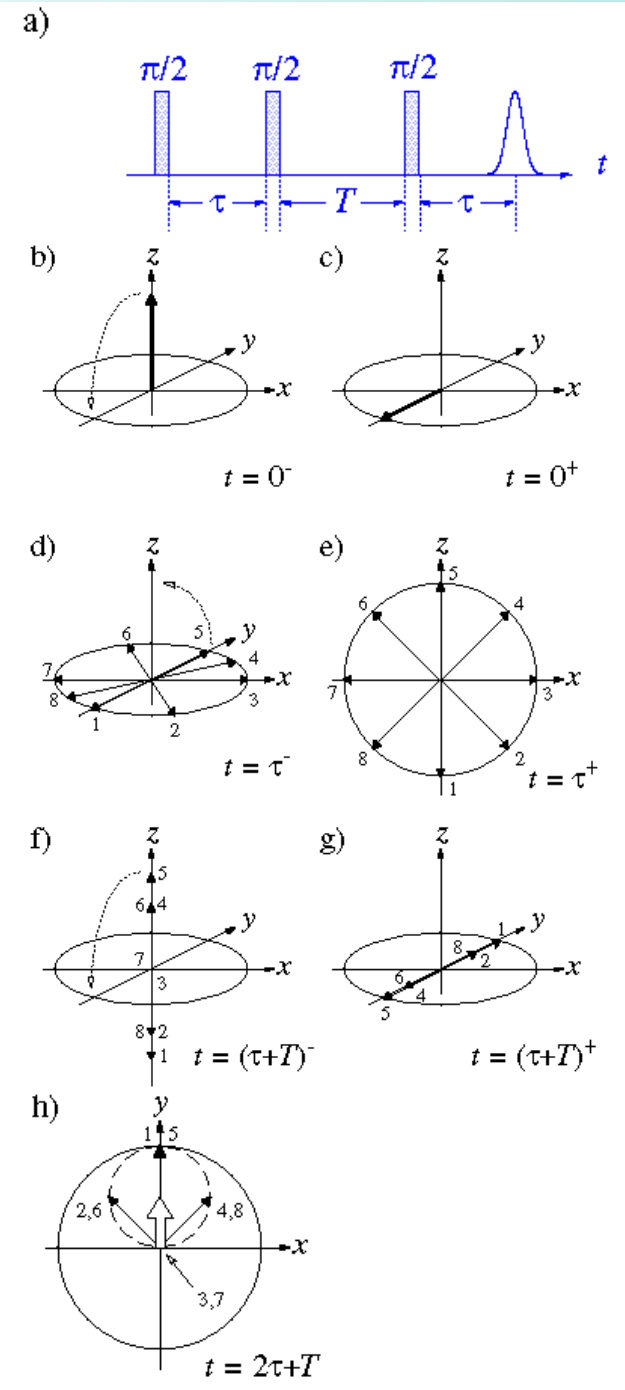
In a two-pulse ESEEM experiment, time $\tau$ between the two pulses is increased and the decay of the primary echo is monitored. The echo decays due to spin-spin and spin-lattice relaxation. Fourier transformation of the time-domain modulation pattern yields a spectrum with frequencies directly related to the hyperfine and nuclear quadrupole interactions.

The decay of the echo caused by the spin-spin relaxation time $T_2$, which is in most cases of the order of a few microseconds, is usually a serious drawback, i.e. the echo cannot be followed for a sufficient long time. This problem can be overcome by using a three-pulse sequence, which selects for the slower $T_1$ relaxation.
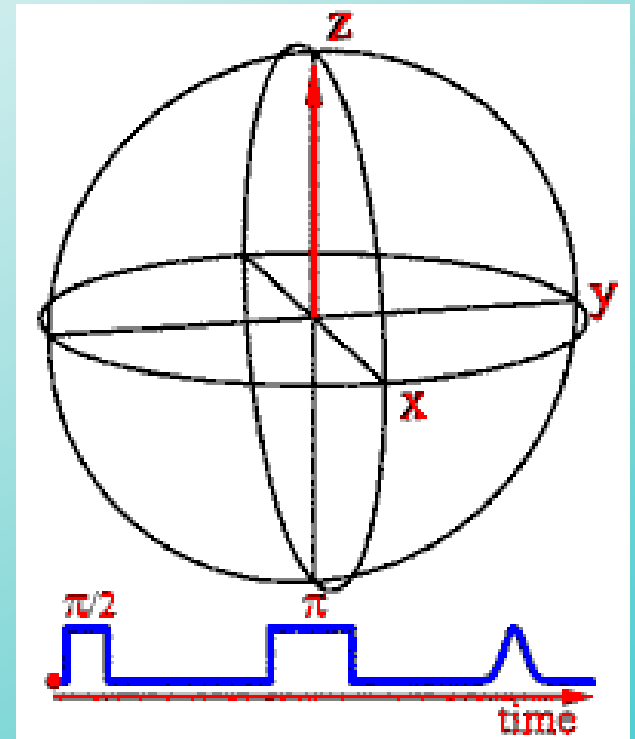
The three-pulse sequence, $\pi/2$-$\tau$-$\pi/2$-T-$\pi/2$-$\tau$-echo (right, a) creates a stimulated echo at time $\tau$ after the third $\pi/2$ pulse. The equilibrium z-magnetization (b) is transferred to transverse magnetization (x, y-plane) by the first $\pi/2$ pulse delivered in the x-axis (c). During free evolution of length $\tau$, the magnetization dephases (d). The second $\pi/2$ pulse rotates the magnetization vectors into the x,z-plane (e). During time T, the transverse magnetization decays (f). At time t=$\tau$ + T, the third $\pi/2$ pulse transfers the z-magnetization pattern again to transverse magnetization (g), which forms an echo at time t = $2\tau$ + T along the +y-axis. The dotted curve represents the locus of the magnetization vector tips, the open arrow is the stimulated echo (h). The echo here is also a "pancake-like" echo in the x,y-plane, but the population detected is now determined by the $T_1$ relaxation time.

The pulse sequence is similar to the NOESY sequence in pulsed NMR.

In a three-pulse ESEEM experiment, a modulation of the stimulated-echo amplitude is observed, if time T between the second and the third pulse is increased while the time $\tau$ between the first and second pulse is kept constant.

In contrast to the two-pulse ESEEM experiment, the three-pulse ESEEM spectra are free of sum and difference frequencies.

The FID contains information about the coupling to nuclear spins, but the time scale over which these are observed is much longer than with the two pulse sequence. The resolution is limited by the electron spin-lattice relaxation time $T_1$, which is usually much larger than the electronic spin-spin relaxation time $T_2$, which dominates the relaxation in the x,y-plane.
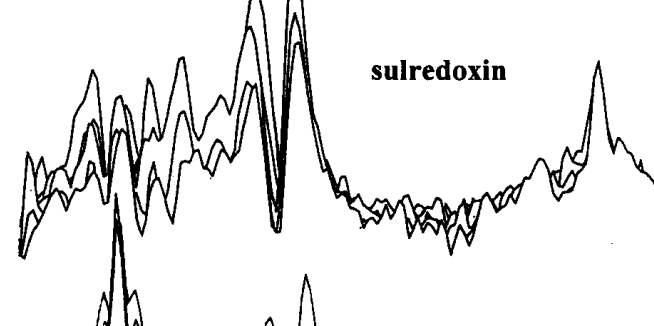
# 2D-stacked-plots of 3-pulse ESEEM data
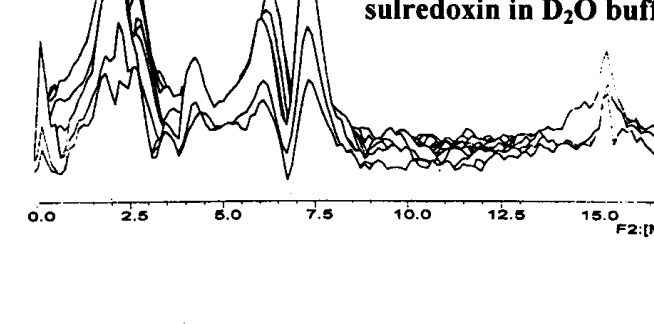


**ESEEM spectra of Rieske-type clusters**
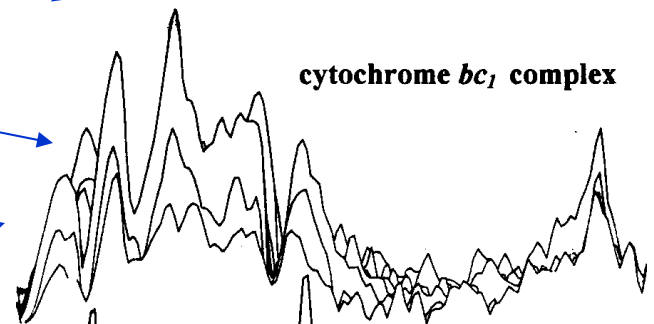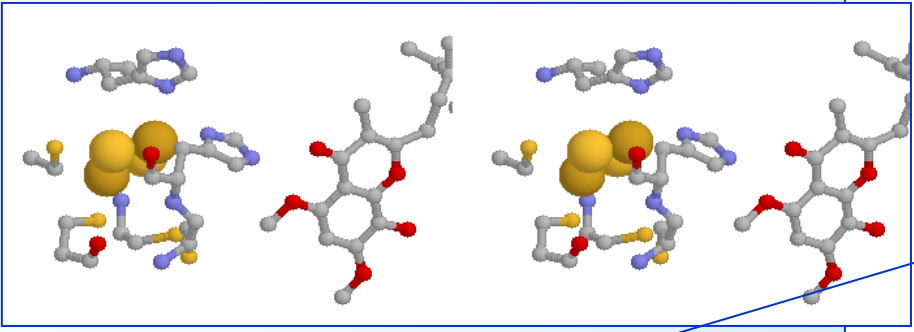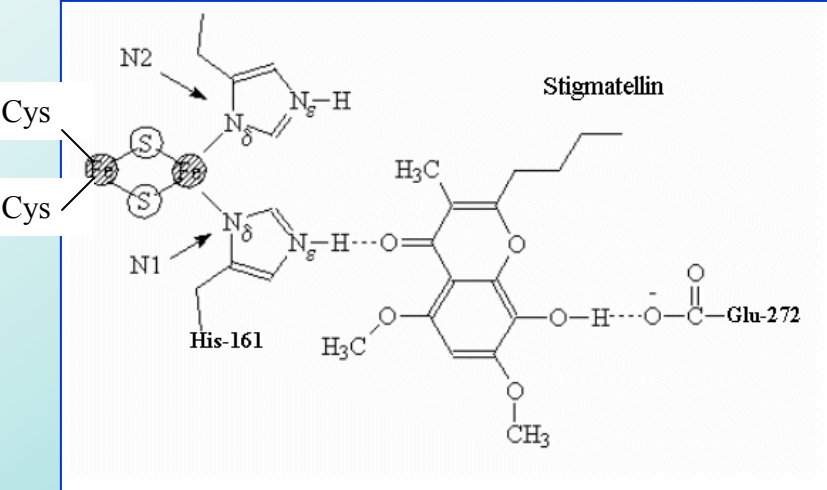
cytochrome $bc_1$ complex
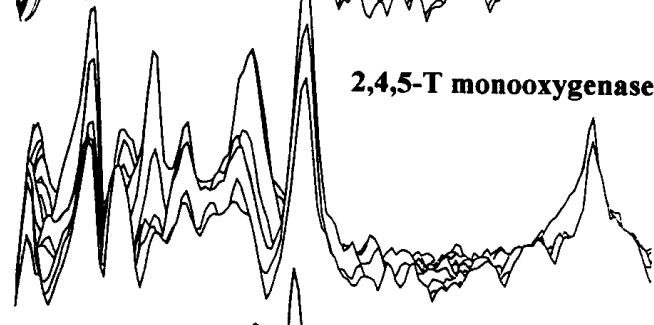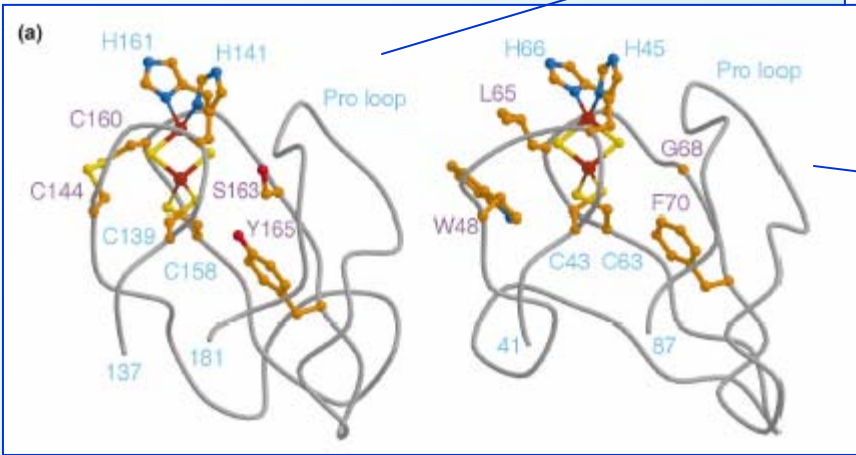
2,4,5-T monooxygenase

sulredoxin

sulredoxin in $D_2O$ buffer

Stigmatellin

His-161

Cys

Cys

**Use of ESEEM to explore orientation of a paramagnetic center.**

In an ESEEM experiment, the sample is placed in the spectrometer, and the field is adjusted so as to select a particular feature of the spectrum seen in CW-EPR.



Stacked plots from 3-pulse ESEEM

at $g_x$ — quinone, stigmatellin, myxothiazol

at $g_y$

at $g_z$

MHz
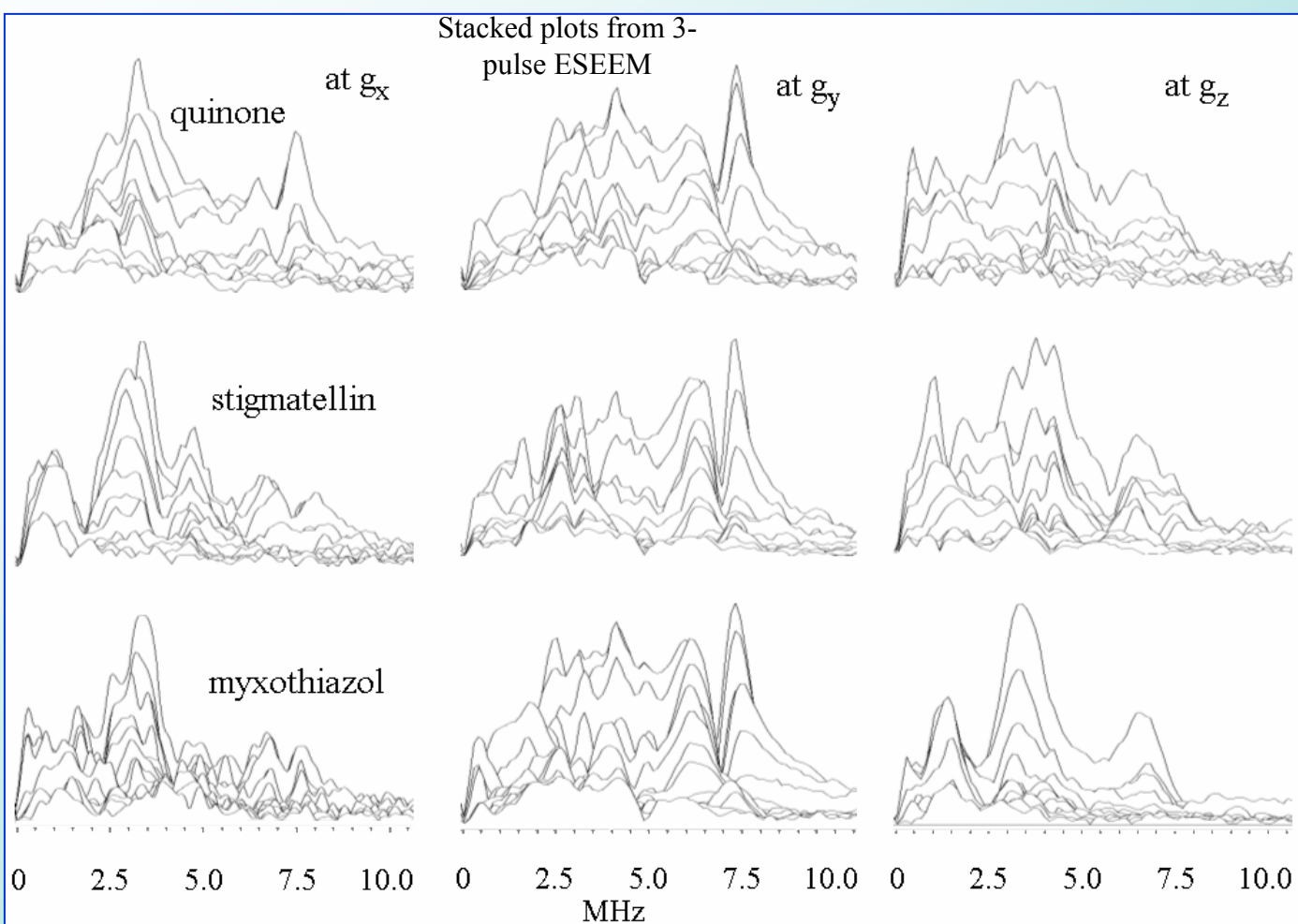
In a rhombic system like the Rieske type [2Fe-2S] centers, this means that one can select a particular orientation, and therefore explore only those nuclear interactions that affect the energy levels of the spin transitions in that orientation.

In this experiment, we see that the spectra of the complex with quinone as ligand to the cluster are similar to those with stigmatellin, but different when no ligand is present (with myxothiazol). This suggests a similar liganding and orientation.

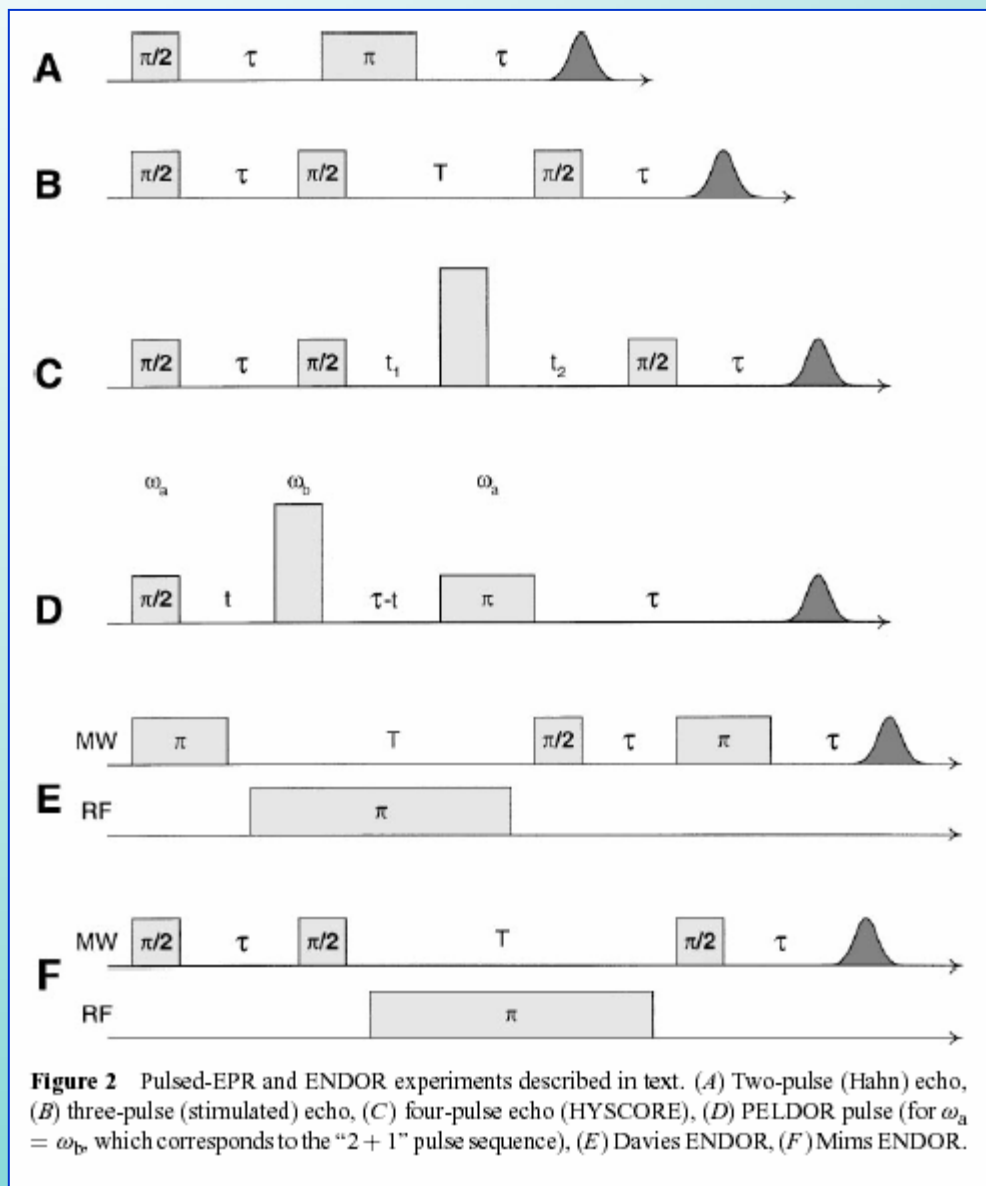HYSCORE (Hyperfine Sublevel Correlation Spectroscopy) is a two-dimensional four-pulse experiment (right) which correlates the two ENDOR frequencies associated with a particular hyperfine coupling. The experiment is based on the three-pulse stimulated echo sequence. A mixing $\pi$ pulse is inserted between the second and the third $\pi/2$ "read" pulse to create correlations between the nuclear spin transitions of the two electron spin manifolds, $m_s$. To acquire the 2D time-domain modulation signal, the stimulated echo amplitude is observed as a function of pulse separations $t_1$ and $t_2$ (with fixed $\tau$). An echo FID is recorded at a series of times for $t_1$ and $t_2$, spectra are obtained by Fourier transform. The two sets of spectra (varying with $t_1$ or $t_2$) are then treated as time domain data and Fourier transformed to give two sets of frequency domain data, which are plotted against each other to generate a contour plot.
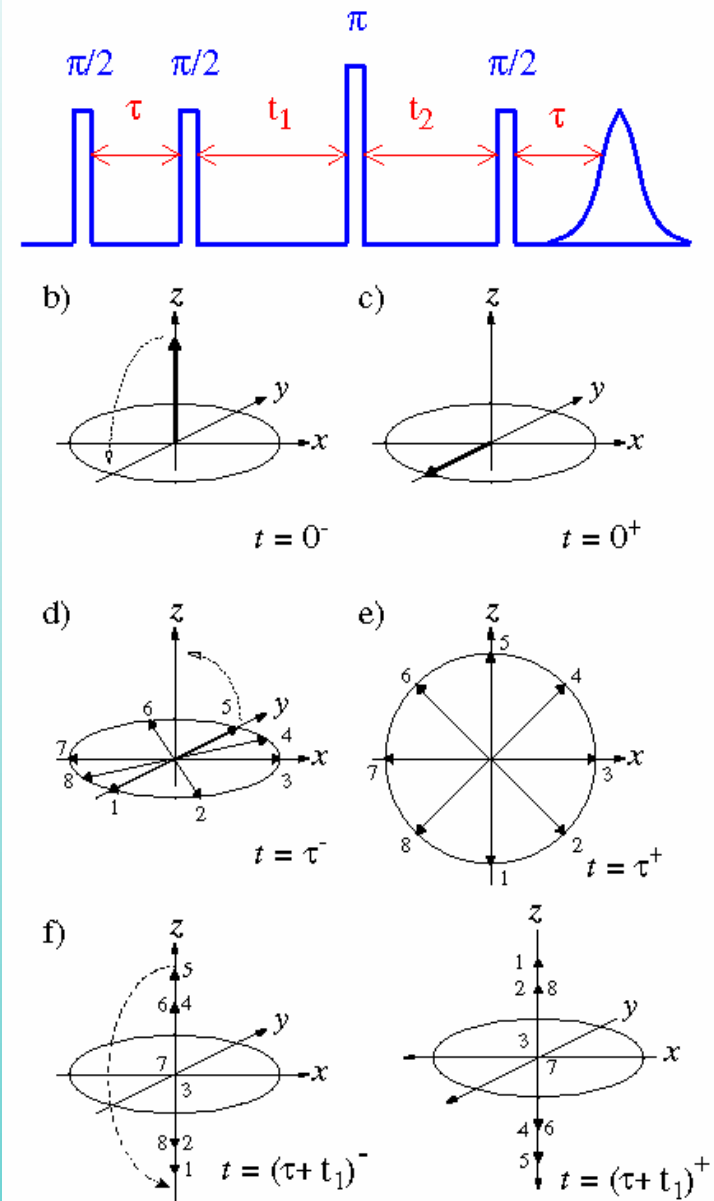
## Summary of pulse sequences for high resolution EPR

Pulse sequences A, B and C are the three we have already discussed. D is a variant with selection by specific frequency.

The last two (E and F) probe the interaction between nuclear and electron spins by observing how a flipping of the nuclear spins using an RF frequency $\pi$ pulse changes the relaxation of the electron spin. This approach is called pulsed-ENDOR, *Electron Nuclear DOuble Resonance* spectroscopy. The microwave pulse sequences are similar to the two-pulse and three pulse sequences of A and B, but with the $\pi$ RF pulse thrown in to flip the nuclear spins.



**Figure 2** Pulsed-EPR and ENDOR experiments described in text. (*A*) Two-pulse (Hahn) echo, (*B*) three-pulse (stimulated) echo, (*C*) four-pulse echo (HYSCORE), (*D*) PELDOR pulse (for $\omega_a = \omega_b$, which corresponds to the "2 + 1" pulse sequence), (*E*) Davies ENDOR, (*F*) Mims ENDOR.

Prisner, T., Rohrer, M. and MacMillan, F. (2001) Pulsed EPR spectroscopy: Biological Applications. Annu. Rev. Phys. Chem. 52, 279–313
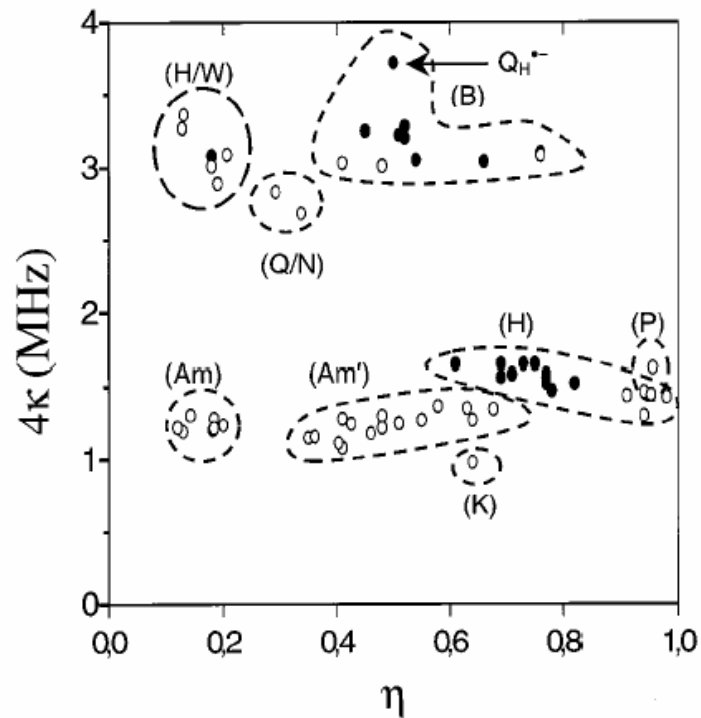
FIGURE 5: Two-dimensional plot of quadrupolar parameters of interacting nitrogens as obtained by $^{14}$N-ESEEM spectroscopy of quinones in different membrane proteins (●) and by $^{14}$N-NQR on model systems (○) (see ref *33* and references therein for $^{14}$N-NQR data). (H/W) Indole, tryptophan, and histidine N($\epsilon$) nitrogen, *18*; (Q/N) glutamine and asparagine NH$_2$ nitrogen; (B) backbone nitrogen, peptide, di- and tripeptide, triglycine, *16, 17, 19*; (Am) and (Am′) NH$_3^+$ amino group nitrogen, (K) NH$_3^+$ lysine nitrogen, (P) proline nitrogen, (H) and histidine N($\delta$) nitrogen, *16, 17, 19*.
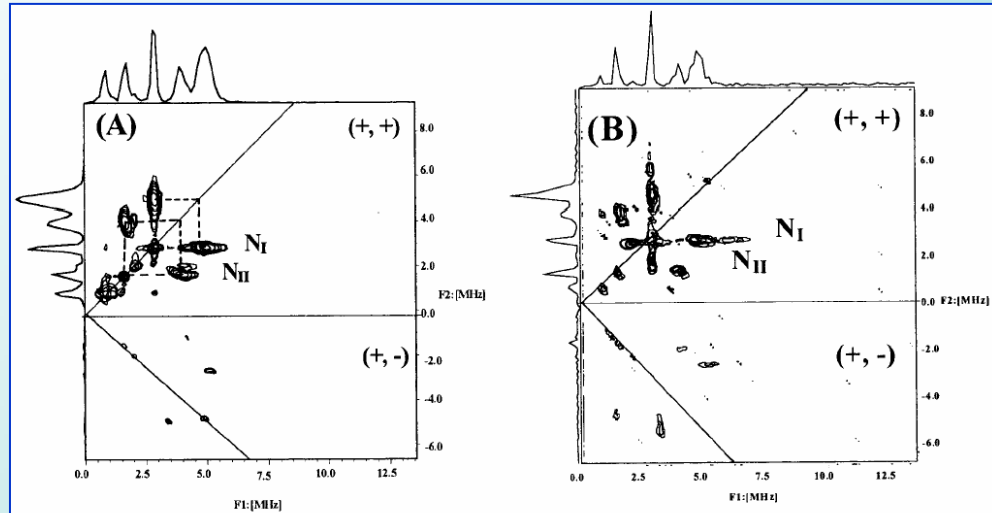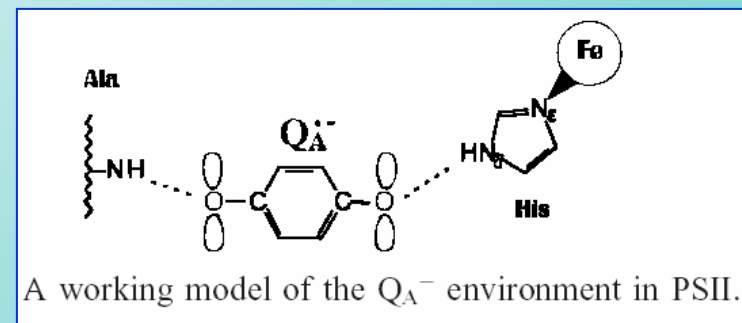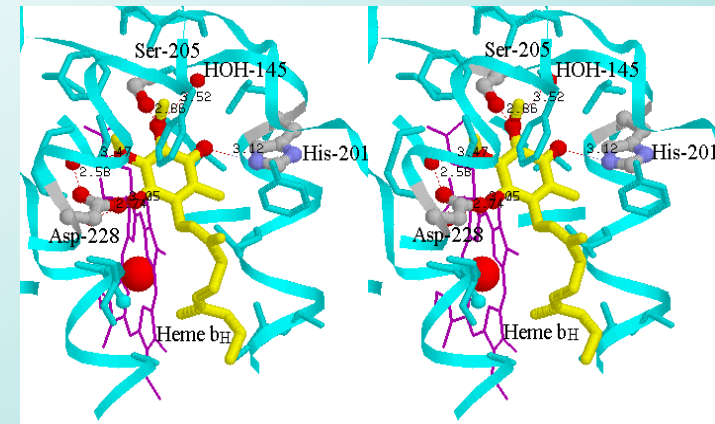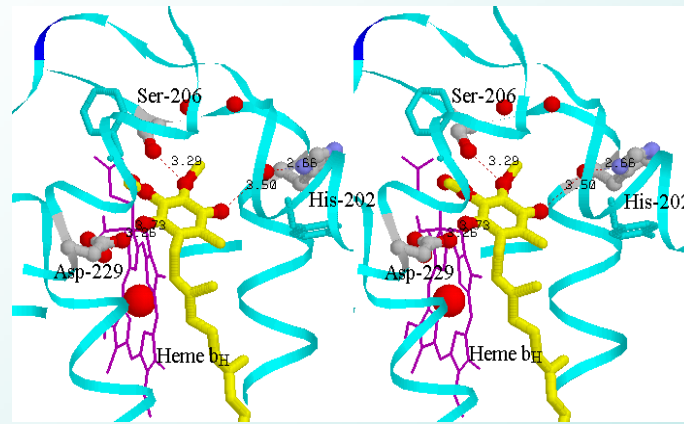


**Figure 5.** Contour plots of 2D-HYSCORE spectra for Q$_A^-$ in pH 11-treated PSII buffered at pH = 9.2 (A) and pH 5.0 (B). Experimental conditions: $H$ = 3457 G; sample temperature, 16 K; $\tau$ = 160 ns; and other conditions as in Figure 2.



A working model of the Q$_A^-$ environment in PSII.

Deligiannakis, Y., Hanley, J. and Rutherford, A.W. (1999) 1D- and 2D-ESEEM Study of the Semiquinone Radical Q$_A^-$ of Photosystem II. *J. Am. Chem. Soc. 121,* 7653-7664

$$\nu_{dq\pm} \approx 2[(\nu_1 \pm \frac{A}{2})^2 + \kappa^2(3+\eta^2)]^{1/2}$$

Grimaldi, S., MacMillan, F., Ostermann, T., Ludwig, B. Michel, H. and Prisner, P. (2001) QH$^{\bullet-}$ ubisemiquinone radical in the *bo$_3$*-type ubiquinol oxidase studied by pulsed EPR and HYSCORE spectroscopy. *Biochemistry 40,* 1037-1043

Recent X-ray structures of the $bc_1$ complex from different groups show a difference in the liganding of the quinone bound at the $Q_i$-site of the complex by a histidine.

Which structure reflects the mechanism?

Pulsed EPR has shown that the histidine is involved as a ligand to semiquinone.



**Structures of the Q-$_i$-site showing different orientations of Q and His-202**, Coordinates from Hunte (1ezv) (left), and from Berry (unpublished 2.1 Å structure, right), with heme $b_H$ in a similar orientation. Stereo pairs for X-eye viewing.

**HYSCORE plot (++ quadrant) for semiquinone at the Q$_i$-site**. The contour plots show a cross-correlation of the [1.7, 3.1] MHz feature (zoomed in the insert) indicating that these lines come from a single N of histidine.
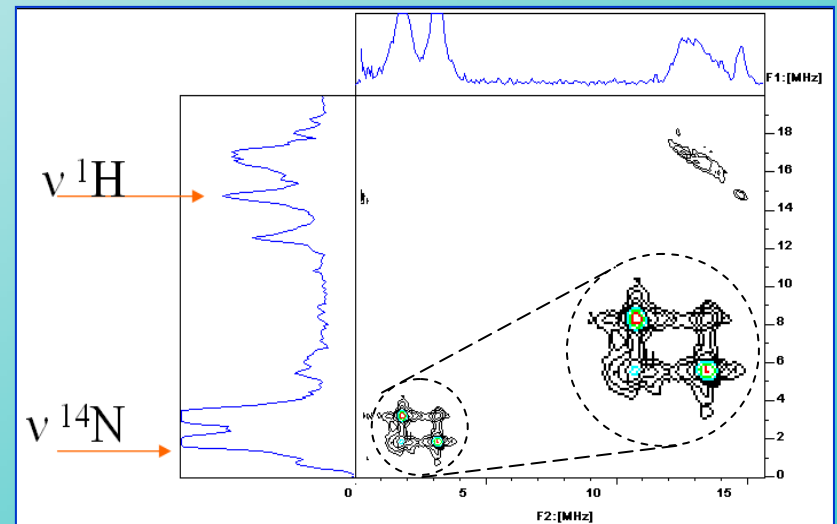
## Take-home messages from EPR

The physics underlying EPR spectroscopy is essentially the same as that for NMR. In practice, there are differences arising from the following:

a) The different energy ranges (microwaves for EPR, RF for NMR), and hence different timescales. This also translates into greater technical difficulty for EPR.

b) The availability of fixed frequency microwave sources requires that spectral sweeps are generated through changes in field.

c) The electron has three components to its magnetic moment, contributed by spin, atomic orbital, and molecular orbital components of angular momentum.

d) The asymmetry of the molecular orbit leads to orientation dependent lines in the EPR spectrum that give rise to spectra in random samples which represent their overlap. Most common spectral envelopes are referred to as isotropic (symmetrical), axial ($g_x=g_y<g_z$, or $g_x=g_y>g_z$), and rhombic ($gx{\neq}gy{\neq}gz$).

e) The separate lines can be measured in oriented samples or crystals, or by selection of lines for pulsed EPR. In the latter approach, the field is selected so that the frequency of the microwave pulse is in resonance with the EPR line of interest.

f) In pulsed EPR, the vector of the spin system is rotated from its equilibrium alignment in the applied field by application of a microwave pulse. The pulses are commonly called $\pi$ (rotation through 180°) and $\pi/2$ (90°) pulses. As the system relaxes back to the equilibrium alignment, it emits photons of microwave frequency corresponding to the interaction energies of the nuclear spins with which the electron spin interacts. The time course of these constitutes the FID (free-induction decay) detected after the pulse. Deconvolution of the FID signal by Fourier transformation to the frequency domain gives a spectrum of the underlying frequencies.

g) The detector picks up signals in the x,y-plane. The purpose of a pulse sequence is to end up with the signal of interest in this plane, but with different times of evolution in either the z-plane ($T_1$ components, in 3-pulse EPR, or HYSCORE) or the x,y-plane ($T_2$ components, in 2-pulse EPR). The $T_2$ components decay more rapidly than $T_1$, and the latter therefore can potentially give more information.

h) The spectra generated by pulsed EPR can provide useful information about the local structural environment. At natural abundance, the spectra are dominated by interactions with $^1H$ (H-bonds, local $H_2O$, bonded H, etc.) and by $^{14}N$ (backbone N, histidine ring N, etc.). Isotopic substitution can provide additional information.

i) Analysis of the spectra can provide distances and torsional angles, and hence structural detail. The range of interaction is <~5-6 Å.